

Testing snow water equivalent retrieval algorithms for passive microwave remote sensing in an alpine watershed of western Canada

Jinjun Tong, Stephen J. Déry, Peter L. Jackson, and Chris Derksen

Abstract. Brightness temperatures (TBs) from the special sensor microwave imager (SSM/I) and advanced microwave scanning radiometer (AMSR-E) from 2003 to 2007 are utilized to retrieve and evaluate the snow water equivalent (SWE) over the complex terrain of the Quesnel River Basin (QRB), British Columbia, Canada. Various algorithms including the Environment Canada (EC) algorithms, the spectral polarization difference (SPD) algorithm, and an artificial neural network (ANN) for both SSM/I and AMSR-E are evaluated against in situ SWE observations using several statistical metrics. The results show that the EC algorithms developed specifically for the southern prairies and boreal forest perform poorly across the complex topography and generally deep snow of the QRB. For other frequency combinations of SSM/I and AMSR-E measurements, significant relationships between TB difference and in situ SWE exist only when the snow accumulation is less than a threshold of 250 or 400 mm, which varies at the different in situ stations. Overall, AMSR-E provides better estimates of retrieved SWE than SSM/I. Compared to the algorithms based on TB difference, the ANNs for SSM/I and AMSR-E perform much better. The ANNs trained with all channels of AMSR-E have the best performance in fitting SWE and are able to resolve the temporal variations of SWE at all in situ stations. However, due to the complexity of the topography and vegetation in this mountainous watershed, the ANNs based only on limited in situ stations are not able to retrieve the spatial variations of SWE in this area.

Résumé. Les températures de radiance des capteurs « Special Sensor Microwave Imager » (SSM/I) et « Advanced Microwave Scanning Radiometer » (AMSR-E) de 2003 à 2007 sont utilisées pour estimer et évaluer l'épaisseur équivalente en eau (EEE) de la neige dans le bassin versant de la rivière Quesnel, en Colombie-Britannique, Canada. Une variété d'algorithmes, dont ceux d'Environnement Canada (EC), de la différence spectrale polarisée et d'un réseau artificiel de neurones (RAN) pour SSM/I et AMSR-E, sont évalués contre des données prises sur le champ de l'accumulation en neige utilisant plusieurs statistiques. Les résultats démontrent que les algorithmes par EC pour les prairies et les forêts boréales du Canada performent d'une façon insatisfaisante pour la topographie complexe et la neige abondante du bassin versant de la Rivière Quesnel. Pour d'autres combinaisons de données de SSM/I et AMSR-E, des relations significatives entre les températures de radiance et l'accumulation en neige existent seulement lorsque celle-ci ne dépasse pas soit 250 mm EEE ou 400 mm EEE, dépendant de l'endroit. En général, AMSR-E donne de meilleurs estimations de l'accumulation en neige que SSM/I. Comparés aux algorithmes basés sur une différence de température de radiance, le RAN pour SSM/I et AMSR-E performe beaucoup mieux. Les RANs entraînés avec tous les canaux d'AMSR-E obtiennent les meilleurs résultats en extrayant l'accumulation en neige tout en reconstruisant son évolution temporelle aux stations in situ. Cependant, à cause de la complexité du terrain et de la végétation dans ce bassin versant, les RANs basés sur des données limitées à quelques stations in-situ sont incapables de reconstruire les variations spatiales de l'accumulation en neige dans cet endroit.

Introduction

Snow water equivalent (SWE) is an important parameter in various hydrometeorological systems in northern and high-elevation watersheds (Jain and Lall, 2000; Déry et al., 2004; 2005; Yang et al., 2003; 2007; Dyer, 2008). Global and regional warming have led to changes in snow accumula-

tion, including declines and earlier dates of maximum SWE in North America (Mote et al., 2005; Mote, 2006; Stewart et al., 2005). Significant relationships between SWE and river discharge have been found in the snowmelt-dominated watersheds where the spring freshet dominates the annual hydrological cycle (Stewart et al., 2005; Mote, 2006; Yang et al., 2007; Déry et al., 2005; Barnett et al., 2005).

Received 16 May 2009. Accepted 24 November 2009. Published on the Web at <http://pubservices.nrc-cnrc.ca/cjrs> on 16 July 2010.

J. Tong.¹ Natural Resources and Environmental Studies, University of Northern British Columbia, Prince George, BC V2N 4Z9, Canada.
S.J. Déry and P.L. Jackson. Environmental Science and Engineering Program, University of Northern British Columbia, Prince George, BC V2N 4Z9, Canada.

C. Derksen. Climate Research Division, Environment Canada, Toronto, ON M3H 5T4, Canada.

¹Corresponding author (e-mail: jtong@unbc.ca).

SWE mapping from satellite passive microwave data is an important but difficult goal. A deeper snow cover attenuates the microwave radiation from the snow and underlying ground owing to the scattering effects of snow grains. There is an inverse relationship, therefore, between snow depth and microwave brightness temperature (TB). Normally the TB difference between the 19 and 37 GHz bands is utilized to retrieve the snow depth and SWE (Chang et al., 1987; Goodison and Walker, 1995). However, disagreement can be high between satellite-derived snow depth and ground measurements owing to the coarse spatial resolution of the passive microwave measurements and the simplistic assumptions of empirical retrieval schemes (Tait and Armstrong, 1996). In addition, volume scatter at 37 GHz will not increase when snow depth exceeds about 1 m; meanwhile, standing vegetation absorbs the scattering signal from the underlying snowpack at 37 GHz as well. Therefore, more significant disagreements between in situ measured and passive microwave retrieved SWE have been observed in mountainous areas. Kelly and Chang (2003) also demonstrate that the static parameterization does not work well owing to the heterogeneous nature of snow distributions in the passive microwave pixels.

The special sensor microwave imager (SSM/I) and advanced microwave scanning radiometer (AMSR-E) are comprehensively used to retrieve SWE (Chang et al., 1987; Goodison and Walker, 1995; Derksen et al., 2003; Derksen, 2008). In Canada, the Climate Research Division of Environment Canada (EC) has developed, validated, and applied passive microwave satellite data to the retrieval of snow-covered area (SCA), SWE, and snowpack state for several regions of Canada (Derksen et al., 2003). Since different landscapes affect the microwave radiation in disparate ways, the prairies, boreal forest, and tundra have different algorithms for SWE retrieval. Goodison et al. (1986) developed an empirical algorithm based on airborne microwave radiometer data for mapping SWE in the prairie region of western Canada from SSM/I data. However, algorithms developed for prairie environments are not suitable for forested regions, as they generally underestimate SWE owing to vegetation effects. The vegetation influences not only the snowfall interception and retention on the surface but also the upwelling microwave radiation from the snowpack. Although the relationship between TB and forest inventory variables has been found using high-resolution airborne measurements, coarse-resolution satellite measurements such as SSM/I and AMSR-E are not able to separate the radiation contribution of the snowpack from that of the standing forest (Kurvonen and Hallikainen, 1997). Kelly and Chang (2003) developed a forest bias effect equation to improve the SWE retrieval in nonmountainous areas. Goïta et al. (2003) developed separate algorithms for SWE retrieval from scanning multichannel microwave radiometer (SMMR) and SSM/I for different forest landscapes including deciduous, coniferous, and sparse forest covers. Derksen (2008) extended the SWE retrieval capability to

deeper snow conditions by utilizing 19 and 10 GHz measurements from AMSR-E. Tedesco et al. (2004) successfully trained an artificial neural network (ANN) to retrieve SWE and snow depth from SSM/I in Finland. However, these algorithms have not been evaluated in the forested mountains of western Canada, where the forest coverage ranges from 65% to 90% and the snow depth is much greater than that in other research areas. In this paper, the EC algorithms, various combinations of different channels of SSM/I and AMSR-E, and an ANN based on different channels of SSM/I and AMSR-E are tested and evaluated based on in situ observations of SWE in the Quesnel River Basin (QRB), British Columbia (BC), Canada.

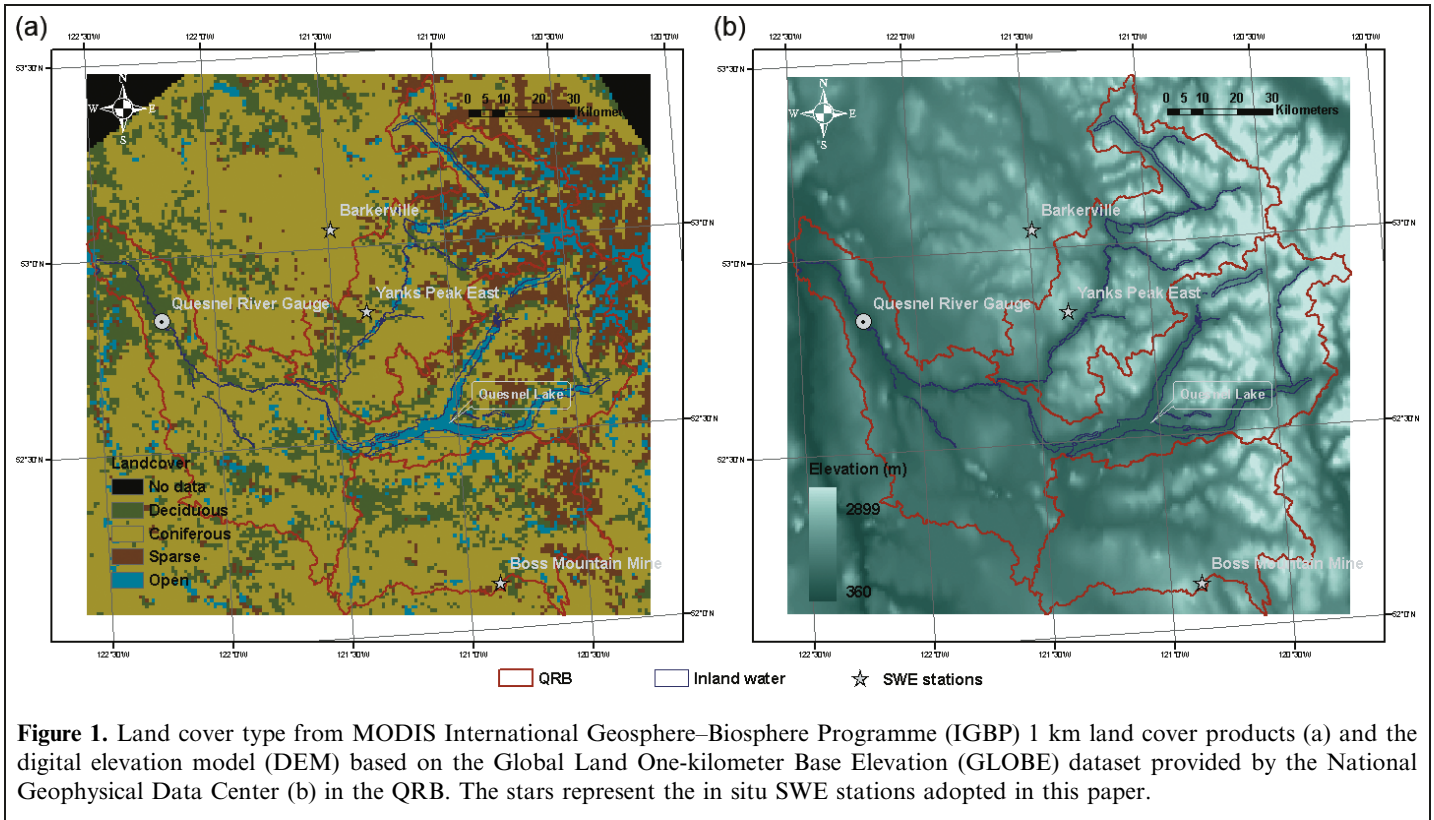
Research area

The QRB, which is one of the 13 main subbasins in the Fraser River Basin, BC, is centred near 52.5°N and 121°W. The QRB covers an area of about 11 500 km², including about 26 equal-area scalable earth-grid (EASE-Grid) cells with a range of topography, meteorological conditions, and land uses across the watershed. Elevation ranges from ~500 m in the western part to 3000 m in the eastern part, with an average elevation of 1375 m. The slopes in the QRB reach a maximum value of 40°. The precipitation across the QRB ranges from 500 to 2500 mm/year, and the annual mean air temperature in the QRB ranges from 1.5 to 7.1 °C (Burford et al., 2009). Three SWE in situ stations operated by the BC Ministry of Environment are located around the QRB. According to the 2004 Moderate-Resolution Imaging Spectroradiometer (MODIS) International Geosphere-Biosphere Programme (IGBP) 1 km land cover products, coniferous forests account for about 64% of the land surface in the QRB, followed by sparse forest with 15%, deciduous forest with 14%, and open area with 7% (**Figure 1**). The coniferous forest covers 70%, 79%, and 96% of the land surface in the EASE-Grid cells that include the three in situ stations of Yanks Peak East (YPE), Boss Mountain Mine (BMM), and Barkerville, respectively (**Figure 2**).

Data

Microwave brightness temperature of SSM/I

The SSM/Is, first launched in June 1987, have been flown on the US Defense Meteorological Satellite Program (DMSP) F-8, F-10, F-11, F-13, F-14, and F-15 to provide continual monitoring of the Earth's surface. The channels of the SSM/I sensor include both horizontally and vertically polarized channels at 19.35, 37.00, and 85.50 GHz and a vertical polarization at 22.235 GHz. Ascending and descending orbit data from SSM/I are available every day and nearly cover the entire globe at 25 km resolution except for some small diamond-shaped areas near the equator and



circular sectors of 2.4° latitude surrounding the north and south poles (Armstrong and Brodzik, 1995). In this paper, the SSM/I Pathfinder daily level 3 north EASE-Grid TB at 25 km resolution from ascending and descending orbits between 2003 and 2007 were downloaded from the National Snow and Ice Data Center (NSIDC) in Boulder, Colorado (<ftp://sidads.colorado.edu/pub/DATASETS/brightness-temperatures/>

polar-stereo/tools/). The original TBs were rescaled into level 3 EASE-Grid TB at 25 km resolution by the National Oceanic and Atmospheric Administration (NOAA) – National Aeronautics and Space Administration (NASA) Pathfinder program (<http://nsidc.org/daac/pathfinder/index.html>).

Microwave brightness temperature of AMSR-E

The AMSR-E is the passive microwave radiometer on board the NASA Aqua platform, launched in May 2002. AMSR-E has both horizontally and vertically polarized channels at 6.925, 10.65, 18.7, 23.8, 36.5, and 89 GHz (www.ghcc.msfc.nasa.gov/AMSR/). The lower frequencies of 6.925 and 10.65 GHz are not available from SSM/I. In addition, AMSR-E has a higher native spatial resolution with 12 km at 36.5 GHz compared with 25 km for SSM/I at 37 GHz. In this paper, the daily AMSR-E north EASE-Grid TB at 25 km resolution from ascending and descending orbits between 2003 and 2007 were downloaded from the NSIDC (<ftp://sidads.colorado.edu/pub/DATASETS/brightness-temperatures/easegrid/amse/>). The NSIDC gridded the original TBs into EASE-Grid TB at 25 km resolution (www.ww.nsidc.org/data/nsidc-0301.html).

In situ meteorological data

There are three in situ observation stations (YPE, BMM, and Barkerville) with automated snow pillows near the QRB that are operated by the Ministry of Environment, BC (see **Table 1** and **Figure 1**). All stations measure snow depth,

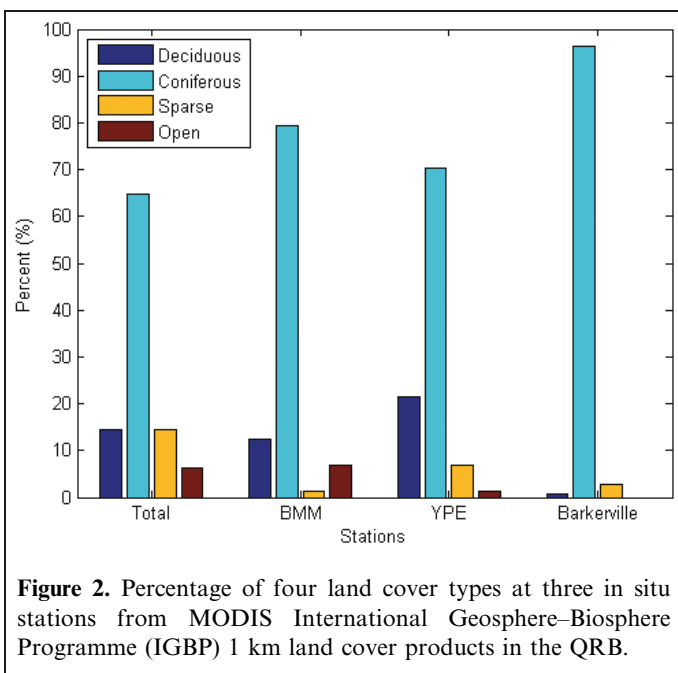


Figure 2. Percentage of four land cover types at three in situ stations from MODIS International Geosphere-Biosphere Programme (IGBP) 1 km land cover products in the QRB.

Table 1. Identification, elevation, coordinates, and annual average maximum SWE of three BC Ministry of Environment snow pillow stations near the QRB.

Station ID	Station name	Lat. (°N)	Long. (°W)	Elev. (m)	Annual avg. max. SWE from 2003 to 2007 (mm)	Avg. elev. in EASE-Grid cell (\pm SD; m)
1C20P	Boss Mountain Mine	52.1	120.8	1460	563	1284 \pm 137
1C41P	Yanks Peak East	52.8	121.3	1670	822	1561 \pm 218
1A03P	Barkerville	53.1	121.4	1520	338	1461 \pm 145

Note: Also included in the table are the average and standard deviation (\pm SD) of elevations in the corresponding 25 km² EASE-Grid cells for the three in situ station sites.

SWE, air temperature, and precipitation on an hourly basis, and the data are available online (<http://a100.gov.bc.ca/pub/aspr/>). Although there is potentially a maximum 10% error in the SWE measured by the snow pillows (S. Jackson and K. Przczek, personal communication, 2009), the snow pillow data over 2003–2007 are taken here as ground validation of SWE in the EASE-Grid cells. The snowpack evolution is strongly controlled by the topography (Tong et al., 2009). The digital elevation model (DEM) based on the Global Land One-kilometer Base Elevation (GLOBE) dataset provided by the National Geophysical Data Center is shown in **Figure 1**. **Figure 3** shows the DEM distribution of the 25 km EASE-Grid cells including the in situ stations and suggests that the elevations of the in situ stations fall within the centre of the distribution in the averaged EASE-Grid cell elevation. Thus the in situ observed SWE may well represent the averaged SWE in the EASE-Grid cells.

Methods

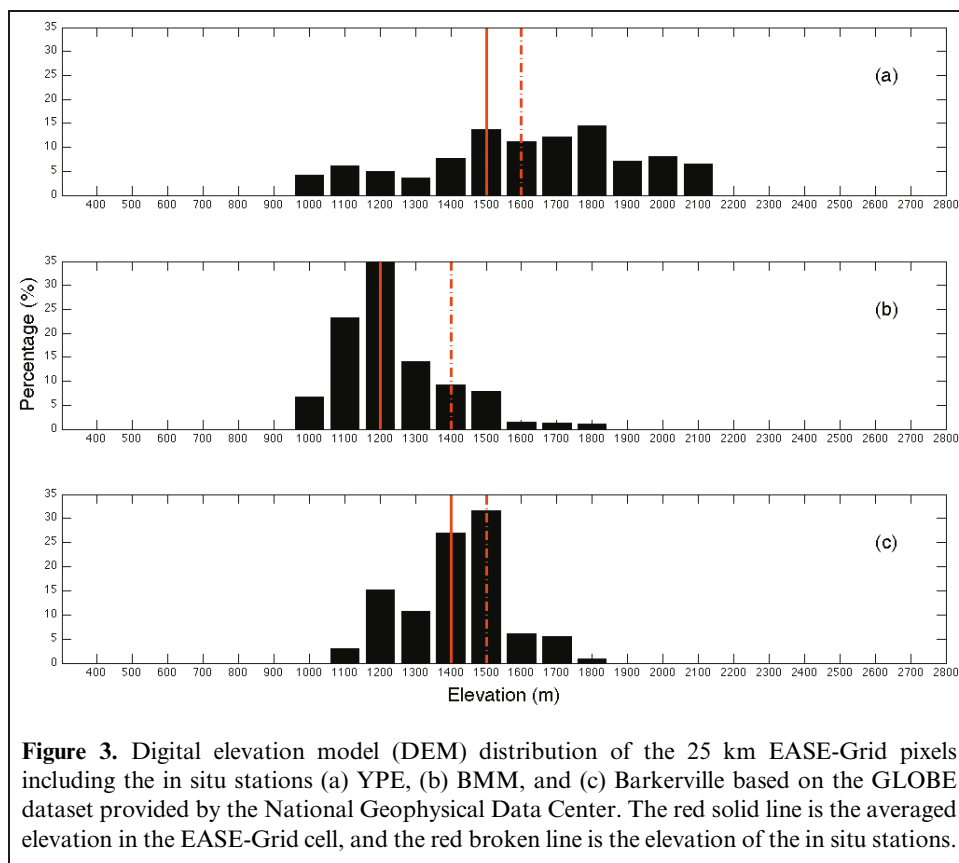
Regressed algorithm based on the TB difference of different channels

Most retrieval algorithms for SWE from microwave remote sensing are based on the TB difference of various channels. The spectral polarization difference (SPD) algorithm was first developed by Aschbacher (1989) to retrieve SWE and was based on the combination of SSM/I channels: 19V, 37V, and 19H (AMSR-E channels 18.7V, 36.5V, and 18.7H). The combination of the channels is as follows:

$$\text{SPD} = [\text{TB}(19\text{V}) - \text{TB}(37\text{V})] + [\text{TB}(19\text{V}) - \text{TB}(19\text{H})] \quad (1)$$

$$\text{SWE} = a\text{SPD} + b \quad (2)$$

where TB (K) is the brightness temperatures of different



channels; and a and b are the coefficients recalculated according to the in situ observed SWE (mm) and TBs with units of millimetres/K and millimetres, respectively. The Chang algorithm was developed to retrieve snow depth based on the TB difference between 19H and 37H of SMMR (Chang et al., 1987). The Chang algorithm used in this paper adopts the TB difference between 19V and 37V for SSM/I and the TB difference between 18.7V and 36.5V for AMSR-E. Since AMSR-E has 10.7H and 10.7V channels, which have proved effective in the retrieval of SWE in forested areas, the TB differences between 36.5V and 10.7V and between 18.7V and 10.7V are adopted to develop retrieval algorithms in our research area as well (Derksen, 2008). The equations are as follows:

$$\text{SWE} = c[\text{TB}(36.5\text{V}) - \text{TB}(18.7\text{V})] + d \quad (3)$$

$$\text{SWE} = e[\text{TB}(36.5\text{V}) - \text{TB}(10.7\text{V})] + f \quad (4)$$

$$\text{SWE} = g[\text{TB}(18.7\text{V}) - \text{TB}(10.7\text{V})] + h \quad (5)$$

where c , d , e , f , g , and h are the coefficients recalculated based on the TB of SSM/I and AMSR-E and the in situ observed SWE (mm) from the YPE, BMM, and Barkerville stations, respectively, with units of millimetres/K for c , e , and g and millimetres for d , f , and h .

Artificial neural network

An ANN is composed of some simple neurons connected by various architectures. An ANN is trained and adjusted based on the input and output data to better perform a particular function. Normally, an ANN includes at least one input layer and one output layer, and there may be some hidden layers between them case by case. An ANN is trained by comparison of the output and the target until they reach an optimal result. An ANN with biases, a sigmoid layer, and a linear output layer can approximate most functions with a finite number of discontinuities. This approach has been widely adopted to resolve various scientific problems including SWE retrieval and the prediction of precipitation, among others (Tedesco et al., 2004; Zhang et al., 2007). Therefore, a feed-forward network that includes an input layer, a nonlinear sigmoid hidden layer, and a linear output layer is adopted to build the connection between the brightness temperatures of AMSR-E and SSM/I and SWE. The neurons in successive layers are fully interconnected with weights controlling the strength of the connections. A back-propagation (BP) algorithm, which is based on the Widrow–Hoff learning rule to multiple-layer networks, is used to train the feed-forward network (Hornik et al., 1989). The BP learning rule adjusts the weights of neurons by minimizing the mean square error (MSE) between the target vectors and network output vectors. The network weights in standard BP are moved along the negative of gradient of the performance

function. The performance of the network mainly depends on the training data.

In our study, different combinations of channels are used to generate the training data to explore their roles in the SWE retrieval. For AMSR-E, there are two combinations of channels: one is the combination of 18.7 and 36.5 GHz vertical and horizontal channels, and the other is a combination of all 12 channels. For SSM/I, there are also two combinations of channels: one is the combination of 19 and 37 GHz vertical and horizontal channels, and the other is the combination of all seven channels. To confirm whether a trained ANN in a set is applicable to others, a single trained ANN based on both the YPE station (with the highest average snow accumulation) and the Barkerville station (with the lowest average snow accumulation) is used to calculate the SWE at the BMM station. In addition, the in situ SWE and TB from 2003 to 2005 are used to train the ANNs; however, the in situ SWE and TB from 2006 to 2007 are adopted to validate the performance of the ANNs. The parameters of networks vary for different training runs to improve the ANN at each test site. A fixed MSE and a maximum number of iterations, which vary case by case, are set to end the ANN. In addition, the early stopping technique is also adopted to stop the ANN training. In this approach, the available data are divided into three subsets, namely a training set, a validation set, and a test set. The training set is used to calculate the gradient and update the network weights and biases. The validation set is used to interrupt the ANN training process by monitoring the error of the ANN applied to that dataset. The validation error normally decreases during the training process; however, the validation error typically begins to rise when overfitting occurs. In this case, the training is terminated, and the weights and biases at the minimum of the validation error are selected. Although the test set error is not used during the training, it is useful to determine the division of the dataset. The division of the dataset is considered poor if the test set error reaches a minimum at a significantly different iteration number than the validation set error.

Data processing and evaluation of algorithms

Since microwave remote sensing cannot detect shallow or wet snow, some methods are adopted to select the dry snow data to improve the algorithm results. For the in situ SWE observations, the days were selected when the maximum temperature was below 0 °C and SWE > 10 mm. For the TB, the diurnal amplitude variation (DAV) methods were used to select the snowmelt days (Ramage et al., 2006). If the absolute value of TB difference of 37V for SSM/I (36.5V for AMSR-E) between ascending and descending orbits at a given day exceeds 10 K, it is considered as a snowmelt day and is not included in the analysis. In addition, only descending data with overpasses during the morning or “cold” period are used to avoid snowmelt effects. To reduce the impacts of atmospheric daily variability on the TBs, a

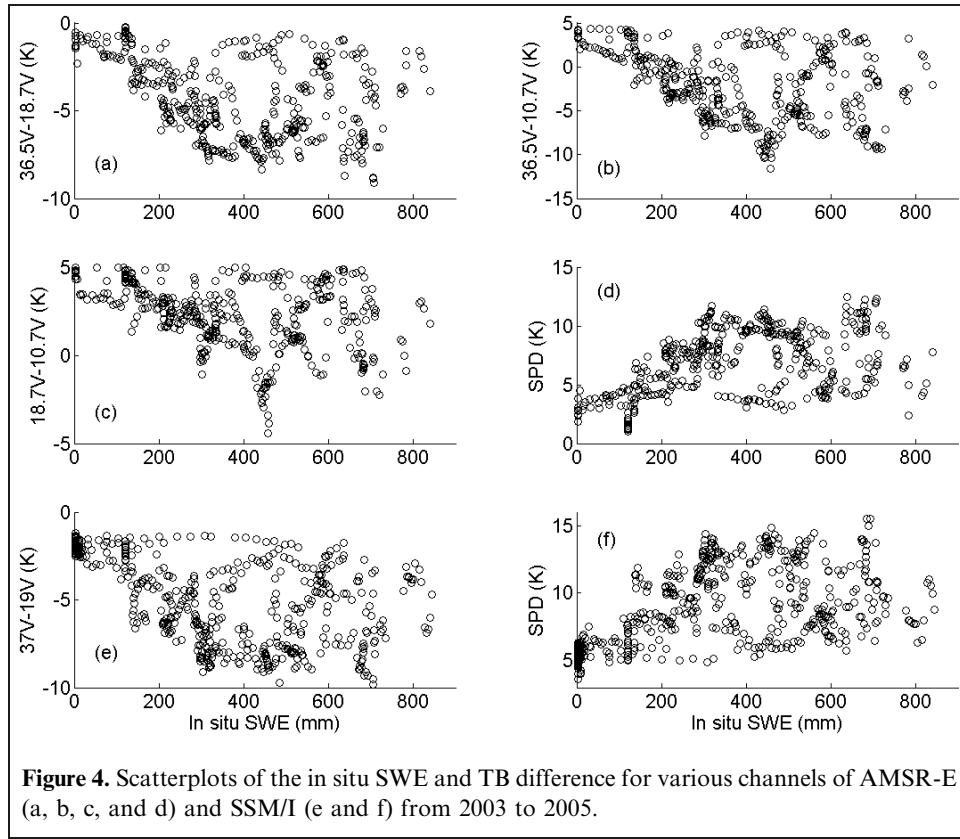


Figure 4. Scatterplots of the in situ SWE and TB difference for various channels of AMSR-E (a, b, c, and d) and SSM/I (e and f) from 2003 to 2005.

5 day moving average was applied to the selected data according to the aforementioned criteria. To evaluate the performance of different algorithms, the root mean square error (RMSE), multiple correlation coefficient (R), and linear regression coefficient (r) are calculated as follows:

$$RMSE = \sqrt{\frac{1}{n} \sum_{i=1}^n [SWE_{pred}(i) - SWE_{true}(i)]^2} \quad (6)$$

$$R = \frac{\sum_{i=1}^n \{ [SWE_{pred}(i) - \overline{SWE_{true}}] [SWE_{true}(i) - \overline{SWE_{true}}] \}}{\sqrt{\sum_{i=1}^n [SWE_{pred}(i) - \overline{SWE_{true}}]^2 \sum_{i=1}^n [SWE_{true}(i) - \overline{SWE_{true}}]^2}} \times 100 \quad (7)$$

$$r = \frac{\sum_{i=1}^n \{ [SWE_{true}(i) - \overline{SWE_{true}}] [SWE_{pred}(i) - \overline{SWE_{pred}}] \}}{\sum_{i=1}^n [SWE_{true}(i) - \overline{SWE_{true}}]^2} \quad (8)$$

where the subscript “pred” implies passive microwave predicted SWE, the subscript “true” denotes in situ observations of SWE, the overbar represents averaged SWE, and n is the number of samples. The algorithm with the lowest RMSE, the highest R , and the r value closest to 1 qualifies as the best algorithm for our research area. In

addition, the absolute agreement (AA) and relative agreement (RA) between the in situ and retrieved SWE are calculated for ANNs of AMSR-E according to following equations:

$$AA(i) = SWE_{pred}(i) - SWE_{true}(i) \quad (9)$$

$$RA(i) = |AA(i)/SWE_{true}(i)| \times 100 \quad (10)$$

Results

Regressed algorithms based on the TB difference of different channels

Owing to the complexity of the vegetation and topography in the QRB, the new coefficients for the retrieval equations were fitted based on the in situ SWE and TB difference of various channel combinations. **Figure 4** shows the scatterplots of the in situ SWE and TB difference for various channel combinations for SSM/I and AMSR-E at the YPE station. Although there are no obvious linear relationships between the in situ SWE and TB difference for all the data, the correlation coefficients between the in situ SWE and TB difference of AMSR-E when SWE < 400 mm are -0.73 ($p < 0.001$), -0.70 ($p < 0.001$), -0.59 ($p < 0.001$), and 0.74 ($p < 0.001$) for 36.5V–18.7V, 36.5V–10.7V, 18.7V–10.7V, and SPD, respectively. For the BMM and Barkerville stations, the absolute value of correlation

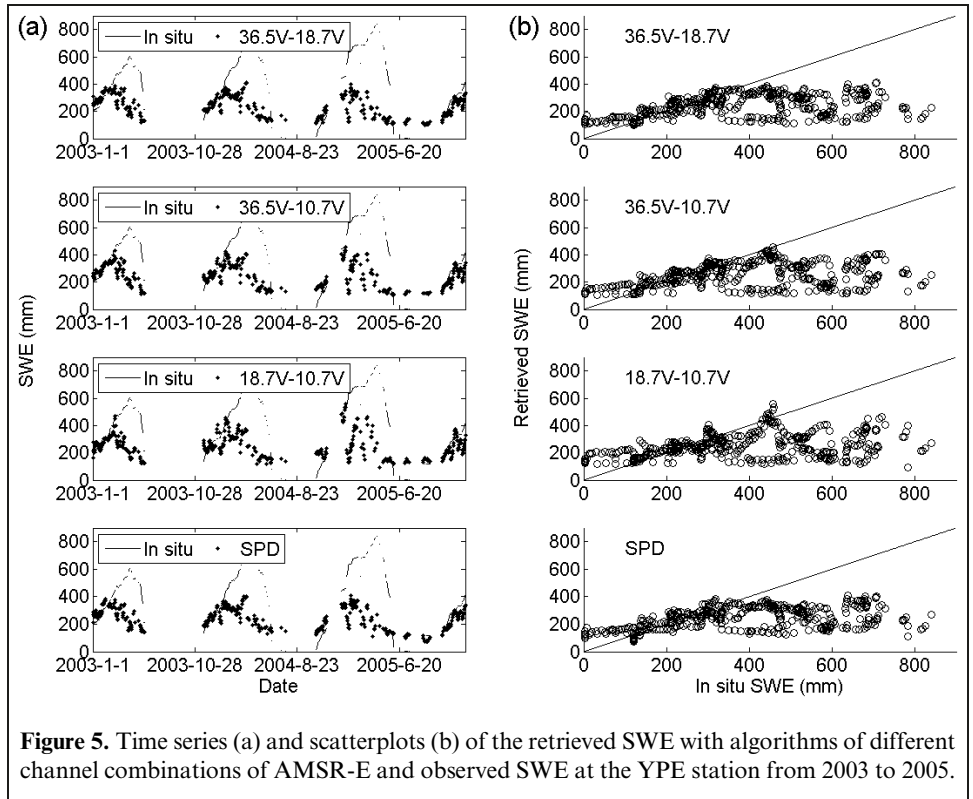


Figure 5. Time series (a) and scatterplots (b) of the retrieved SWE with algorithms of different channel combinations of AMSR-E and observed SWE at the YPE station from 2003 to 2005.

coefficients between the in situ SWE and TB difference for the in situ SWE < 250 mm is greater than 0.6 ($p < 0.001$). Therefore, coefficients for different retrieval equations are fitted based on observed SWE less than 400 mm for the YPE station or 250 mm for the BMM and Barkerville stations. In addition, the maximum TB differences between channels are only 10 K. This is very different from those for the regions where the EC algorithms were developed, where the maximum difference between 37, 19, and 10 GHz may reach 50 K (Derksen et al., 2003; 2005; Derksen, 2008). We also evaluated the EC algorithm in our study area (results not shown). The EC-retrieved SWE does not compare well with the in situ observations at the YPE, BMM, and Barkerville stations. Since the EC algorithm was mainly developed for flatter and less vegetated terrain, the present results indicate it cannot be applied reliably to the complex topography and forested terrain of the QRB.

Figure 5 shows the time series and scatterplots of the in situ and retrieved SWE according to different algorithms from AMSR-E at the YPE station. The statistical results for

the different algorithms from AMSR-E and SSM/I are listed in **Tables 2, 3, and 4**. For the SPD and 37V–19V algorithms of SSM/I, the YPE station shows the best simulated SWE compared to the BMM and Barkerville stations, which exhibit poor performance. This may occur as a result of the lower forest coverage in the EASE-Grid pixel surrounding the YPE station (**Figure 2**). In addition, the 37V–19V algorithm works better than the SPD algorithm at all three stations for SSM/I. For the in situ SWE < 400 mm at YPE, the RMSE, R , and r are 80.71 mm, 78.71%, and 0.62, respectively. For AMSR-E, the SPD, 36.5V–18.7V, and 36.5V–10.7V algorithms outperform the 18.7V–10.7V approach. For the in situ SWE < 400 mm at YPE, the SPD, 36.5V–18.7V, and 36.5V–10.7V algorithms have RMSE, R , and r of about 70 mm, 70%, and 0.5, respectively. Comparing the SPD and 37V–19V algorithms for SSM/I with the SPD and 36.5V–18.7V algorithms for AMSR-E, the AMSR-E performs better than SSM/I at the BMM and Barkerville stations, with an almost similar performance at the YPE station. It is believed that the improved perform-

Table 2. RMSE (mm), R (%), and r for SPD and 36V–18V algorithms for all the in situ SWE and the in situ SWE < 400 mm at the YPE station (<250 mm at the BMM and Barkerville stations) for SSM/I from 2003 to 2005.

Station	SPD, all			SPD < a given SWE (mm)			36V–18V, all			36V–18V < a given SWE (mm)		
	RMSE	R	r	RMSE	R	r	RMSE	R	r	RMSE	R	r
YPE	247.30	30.23	0.23	80.77	78.68	0.62	243.25	32.44	0.24	80.71	78.71	0.62
BMM	198.45	9.61	0.08	65.61	29.79	0.09	193.10	13.12	0.11	64.66	33.90	0.11
Barkerville	83.59	19.23	0.07	59.80	36.27	0.13	82.95	21.61	0.07	59.58	37.15	0.14

Table 3. RMSE (mm), R (%), and r for SPD and 36V–18V, 36V–10V, and 18V–10V algorithms for AMSR-E for all the in situ SWE from 2003 to 2005.

Station	36V–18V			36V–10V			18V–10V			SPD		
	RMSE	R	r	RMSE	R	r	RMSE	R	r	RMSE	R	r
YPE	241.01	15.97	0.13	237.62	17.88	0.15	237.95	17.11	0.14	235.83	18.45	0.15
BMM	155.07	32.57	0.23	160.57	27.89	0.20	169.96	19.49	0.14	154.74	32.59	0.23
Barkerville	81.77	15.87	0.07	83.17	10.94	0.05	84.85	4.72	0.02	82.02	15.66	0.07

Table 4. RMSE (mm), R (%), and r for SPD and 36V–18V, 36V–10V, and 18V–10V algorithms for AMSR-E for the in situ SWE < 400 mm at the YPE station (<250 mm at the BMM and Barkerville stations) from 2003 to 2005.

Station	36V–18V			36V–10V			18V–10V			SPD		
	RMSE	R	r	RMSE	R	r	RMSE	R	r	RMSE	R	r
YPE	70.33	73.52	0.54	73.42	70.65	0.50	83.29	59.62	0.36	70.04	73.77	0.54
BMM	65.53	60.53	0.37	65.02	61.34	0.38	67.62	57.04	0.33	63.83	63.16	0.40
Barkerville	44.60	36.64	0.13	45.72	30.04	0.09	47.01	19.47	0.04	44.18	38.76	0.15

ance could be due to different instrument characteristics such as improved native spatial resolution and light difference of the channel frequency in the AMSR-E 36.5 GHz compared with that in the SSM/I 37 GHz.

Artificial neural networks with different combinations of channels

The in situ SWE and remotely sensed TB from SSM/I and AMSR-E were used to train the ANN at the three different stations. Two combinations of channels were adopted for

SSM/I: one is 37H, 37V, 19H, and 19V; the other includes all seven channels. **Figure 6** shows the in situ and retrieved SWE with an ANN based on four channels and all channels for SSM/I at the BMM station (for brevity, similar figures for YPE and Barkerville are not shown here). The statistical coefficients for retrieved SWE with the ANN for the three stations from SSM/I are listed in **Table 5**. The results show that ANNs based on four channels or all channels of SSM/I obtained similar statistical coefficients at the YPE and BMM stations. However, ANNs based on all channels of SSM/I perform better than those based on the four channels of SSM/I.

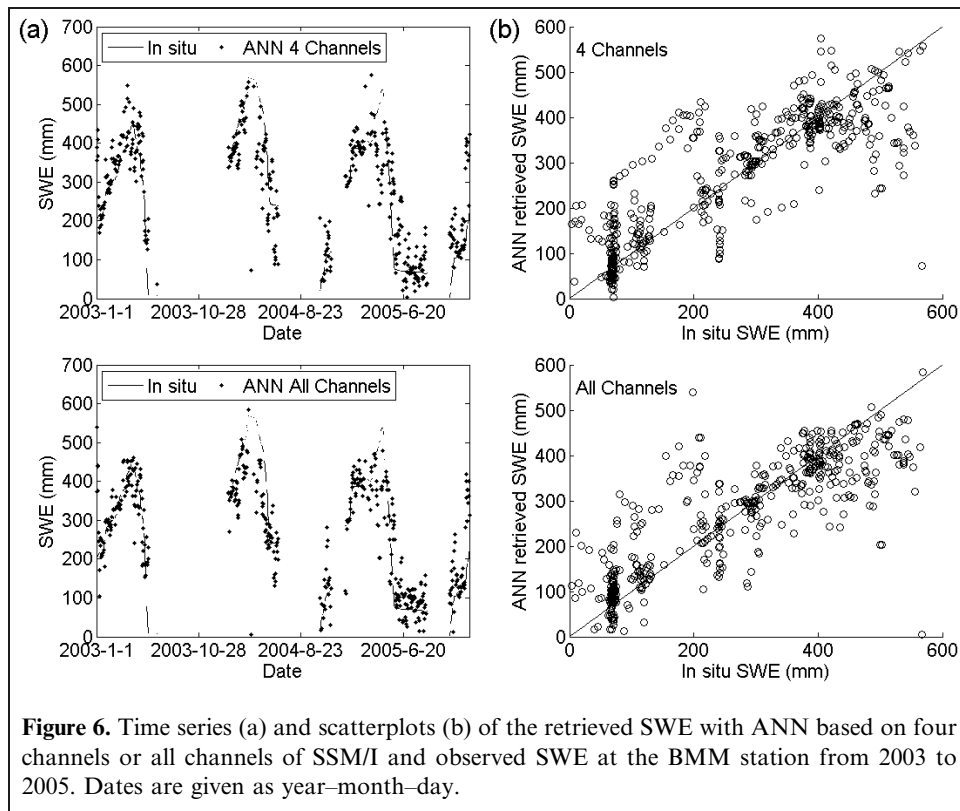
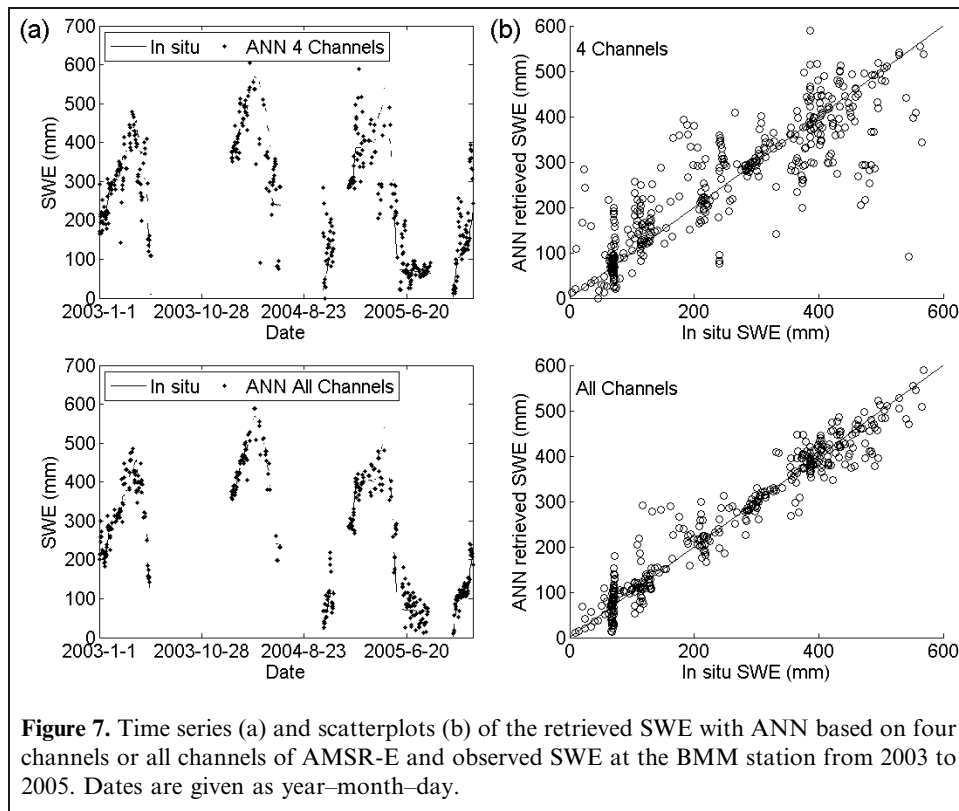


Table 5. RMSE (mm), R (%), and r for ANNs with four channels or all channels of SSM/I and AMSR-E from 2003 to 2005.

Station	AMSR-E						SSM/I					
	ANN, all channels			ANN, four channels			ANN, all channels			ANN, four channels		
	RMSE	R	r	RMSE	R	r	RMSE	R	r	RMSE	R	r
YPE	82.27	91.32	0.93	122.45	79.37	0.68	140.66	79.69	0.65	136.92	80.89	0.66
BMM	45.69	95.49	0.95	76.38	86.66	0.81	87.68	83.01	0.69	89.60	82.36	0.72
Barkerville	36.18	88.65	0.79	67.79	58.18	0.48	60.04	71.38	0.64	68.49	59.03	0.41

Two combinations of channels were adopted for AMSR-E: one is 36.5H, 36.5V, 18.7H, and 18.7V; and the other includes all 12 available channels. **Figure 7** shows the in situ and retrieved SWE with the ANN based on four channels and all channels for AMSR-E at the BMM station. The statistical coefficients for retrieved SWE with ANN for the three stations from AMSR-E are listed in **Table 5**. The results show that the ANNs based on all channels perform much better than those based on only four channels. The RMSE, R , and r of ANN based on all channels at the BMM station are 45.69 mm, 95.48%, and 0.95, respectively, which suggests that the ANN can be used to reconstruct the temporal SWE with a high degree of accuracy. A comparison of results shows that the ANNs based on four channels of AMSR-E perform better than those based on four channels of SSM/I, with a difference in r of about 0.5–0.8 higher at the three stations. Furthermore, the ANNs based on all channels of AMSR-E perform much better than those based on all channels of SSM/I.

To evaluate what degree ANNs can retrieve SWE based on new TBs, the ANNs that are based on all AMSR-E channels were used to retrieve this variable from 2006 to 2007. In the retrieved SWE, some obvious errors such as $SWE < 0$ mm and $SWE > 1200$ mm at the YPE station ($SWE > 800$ mm at the BMM station; $SWE > 600$ mm at the Barkerville station) ranging from 2%–5% of the data were screened. **Figure 8** shows the in situ and retrieved SWE and the scatterplots between them. **Table 6** lists the values of the coefficients of RMSE, R , and r . Compared with the performance of ANNs with trained data, the coefficients of ANNs based on new SWE from 2006 to 2007 are weaker. **Table 7** lists the detailed statistics for the retrieved SWE based on the absolute and relative agreements between in situ and retrieved SWE. The correlation coefficients between in situ and retrieved SWE show a significant relationship ($p < 0.001$), with 0.29, 0.24, and 0.55 for the YPE, BMM, and Barkerville stations, respectively. The retrieved SWE with $AA < 50$ mm accounts for about



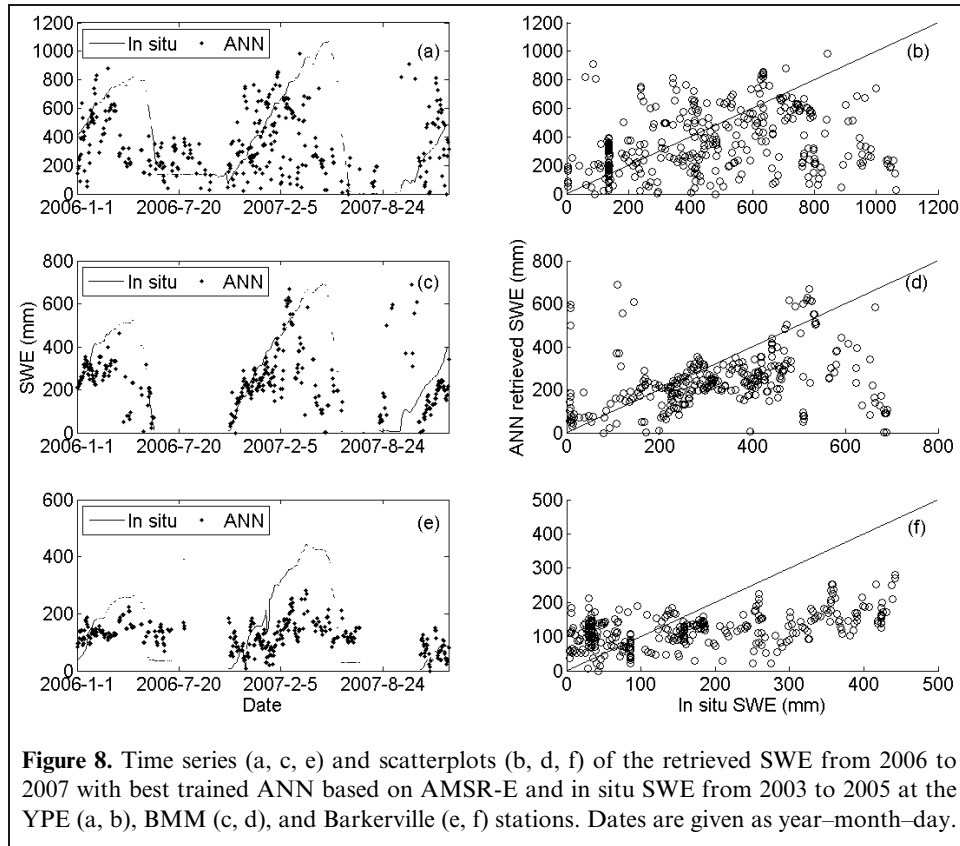


Figure 8. Time series (a, c, e) and scatterplots (b, d, f) of the retrieved SWE from 2006 to 2007 with best trained ANN based on AMSR-E and in situ SWE from 2003 to 2005 at the YPE (a, b), BMM (c, d), and Barkerville (e, f) stations. Dates are given as year–month–day.

13.58%, 23.52%, and 32.93% among all values for YPE, BMM, and Barkerville, respectively, whereas the retrieved SWEs with RA < 50 mm make up about 28.09%, 36.90%, and 22.36% of the total values at YPE, BMM, and Barkerville, respectively. Similar testing for the standard AMSR-E algorithm 36.5V–18.7V has been conducted (results not shown); however, this algorithm does not perform well predicting the SWE from 2006 to 2007 because of the limitations associated with passive microwave remote sensing of deep snow. To evaluate to what degree the ANNs can be used at different in situ stations, the ANN that is trained with the in situ SWE at the YPE and Barkerville

Table 6. RMSE (mm), *R* (%), and *r* for ANNs with all channels of AMSR-E that are used to retrieve the SWE from 2006 to 2007.

Station	RMSE	<i>R</i>	<i>r</i>
YPE	299.26	25.98	0.24
BMM	208.09	17.99	0.20
Barkerville	141.85	24.23	0.23

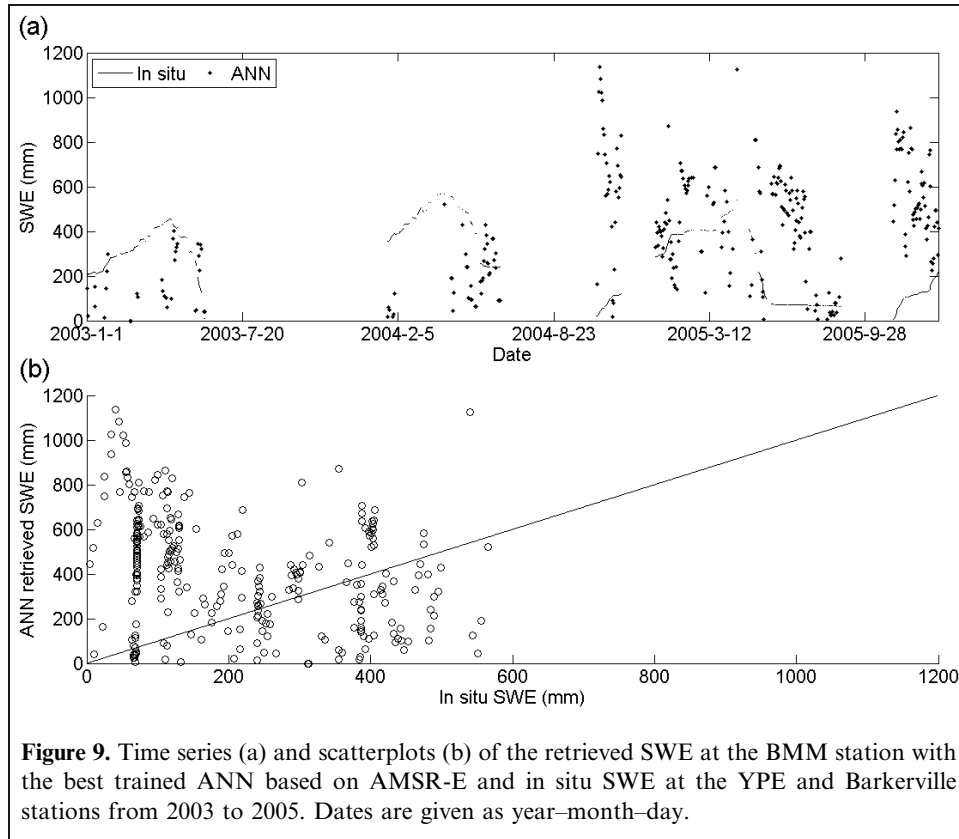
stations from 2003 to 2005 was utilized to retrieve the SWE at the BMM station from 2003 to 2005 (**Figure 9**). The statistical coefficients for the ANN and retrieval performance are listed in **Table 8**. The results show that ANNs trained at given in situ stations perform unsatisfactorily at other locations because of the different land surface characteristics.

Discussion and conclusions

Various snow water equivalent (SWE) retrieval algorithms from the advanced microwave scanning radiometer (AMSR-E) and special sensor microwave imager (SSM/I) were tested based on the in situ SWE over the complex terrain of the Quesnel River Basin (QRB). Although the three in situ SWE stations are only fixed point measurements, they were adopted to represent the SWE in their corresponding EASE-Grid cell. The averaged elevation and the standard deviation of the elevation in the EASE-Grid cells that include the in-situ stations are listed in **Table 1**.

Table 7. Comparison between ANN-retrieved SWE based on all channels of AMSR-E and in situ SWE from 2006 to 2007.

Station	<i>r</i>	Max. of AA (mm)	Min. of AA (mm)	Max. of RA (%)	Min. of RA (%)	Percent of AA < 50 mm	Percent of RA < 25%
YPE	0.29	841.46	1.35	1240.62	0.37	13.58	28.09
BMM	0.24	685.19	0.73	532.50	0.32	25.52	36.90
Barkerville	0.55	298.58	0.11	172.42	0.13	32.93	22.36



The results show that differences between the elevation at the in situ stations and the corresponding EASE-Grid point are only about 100 m, with a standard deviation of 150 m. Therefore, fixed point in situ SWE measurements at the YPE, BMM, and Barkerville stations may well represent the averaged SWE in the whole EASE-Grid cell. In addition, snow measurement stations are very sparse in remote, northern areas such as British Columbia; insufficient in situ observations challenge most of the SWE retrieval research from remote sensing. For instance, only six in situ snow observation sites were suitable for evaluation of the Environment Canada (EC) algorithms in the Mackenzie River Basin, which covers about 1.8 million km² (Derksen et al., 2003). Similarly, only 12 in situ stations were adopted to develop and evaluate various SWE retrieval algorithms in Finland over an area of ~350 000 km² (Tedesco et al., 2004).

The spectral polarization difference (SPD) and other algorithms based on brightness temperature (TB) difference do not perform well in the QRB owing to the dense vegetation and topography. If only the SWE less than

Table 8. RMSE (mm), *R* (%), and *r* for ANN trained with all channels of AMSR-E at the YPE and Barkerville stations from 2003 to 2005 and the RMSE (mm), *R* (%), and *r* for retrieved SWE at the BMM station with the trained ANN at the other two stations.

Station	RMSE	<i>R</i>	<i>r</i>
YPE and Barkerville	81.49	91.80	0.87
BMM	348.71	-22.41	-0.44

400 mm at the YPE station and 250 mm at the BMM and Barkerville stations, which consist of about 70%, 65%, and 93% of the total in situ SWE, respectively, are considered, the SPD and other algorithms based on TB difference perform better. For all the algorithms, the SPD and 36.5V–18.7V algorithms for AMSR-E perform best according to the statistical coefficients. However, the accuracy remains insufficient for the algorithms to be used in the SWE retrieval for the area.

Artificial neural networks (ANNs) with two different combinations of various channels were trained based on the in situ SWE for AMSR-E and SSM/I. ANNs perform much better than the algorithms based on TB differences between various channels. ANNs based on all the channels of AMSR-E perform much better than other ANNs of AMSR-E and SSM/I. The root mean square error (RMSE), multiple correlation coefficient (*R*), and linear regression coefficient (*r*) of the ANNs based on all channels of the AMSR-E are almost 40 mm lower, 20% higher, and 0.3 higher, respectively, than those of the other ANNs of AMSR-E and SSM/I.

To summarize, the retrieval algorithms of SWE based directly on TB difference are not feasible even though the new coefficients for the algorithms were refitted according to in situ observations in the complex terrain of the QRB. The ANNs are able to retrieve the temporal variations of SWE at a given station, especially those based on all channels of AMSR-E. Therefore, the 10.7 GHz channel is very helpful to retrieve the SWE in mountainous forests.

However, due to the complexity of the topography and vegetation in the area, the ANNs based simply on limited in situ stations are not able to retrieve the SWE in other pixels in this region.

Acknowledgments

This research was supported by the Natural Sciences and Engineering Research Council of Canada (NSERC), the Canada Research Chair program of the Government of Canada (S. Déry), and an NSERC Discovery Grant (C. Derksen). Three anonymous reviewers and Dr. Richard Kelly are thanked for their constructive comments on this paper. This is Contribution 7 in the Quesnel River Research Centre Publication Series.

References

- Armstrong, R., and Brodzik, M. 1995. An Earth-gridded SSM/I data set for cryospheric studies and global change monitoring. *Advanced Space Review*, Vol. 16, No. 10, pp. 155–163.
- Aschbacher, J. 1989. *Land surface studies and atmospheric effects by satellite microwave radiometry*. Ph.D. thesis dissertation, University of Innsbruck, Innsbruck, Austria.
- Barnett, T.P., Adam, J.C., and Lettenmaier, D.P. 2005. Potential impacts of a warming climate on water availability in snow-dominated regions. *Nature (London)*, Vol. 438, pp. 303–309. doi:10.1038/nature04141.
- Burford, J.E., Déry, S.J., and Holmes, R.D. 2009. Some aspects of the hydroclimatology of the Quesnel River Basin, British Columbia, Canada. *Hydrological Processes*, Vol. 23, pp. 1529–1536. doi:10.1002/hyp.7253.
- Chang, A.T.C., Foster, J.L., and Hall, D.K. 1987. Nimbus-7 SMMR derived global snow cover parameters. *Annals of Glaciology*, Vol. 9, pp. 39–44.
- Derksen, C. 2008. The contribution of AMSR-E 18.7 and 10.7 GHz measurements to improved boreal forest snow water equivalent retrievals. *Remote Sensing of Environment*, Vol. 112, pp. 2701–2710.
- Derksen, C., Walker, A., and Goodison, B. 2003. A comparison of 18 winter seasons of in situ and passive microwave-derived snow water equivalent estimates in Western Canada. *Remote Sensing of Environment*, Vol. 88, pp. 271–282.
- Derksen, C., Walker, A., and Goodison, B. 2005. Evaluation of passive microwave snow water equivalent retrievals across the boreal forest/tundra transition of western Canada. *Remote Sensing of Environment*, Vol. 96, pp. 315–327.
- Déry, S.J., Crow, W.T., Stieglitz, M., and Wood, E.F. 2004. Modeling snow-cover heterogeneity over complex Arctic terrain for regional and global climate models. *Journal of Hydrometeorology*, Vol. 5, pp. 33–48.
- Déry, S.J., Salomonson, V.V., Stieglitz, M., Hall, D.K., and Appel, I. 2005. An approach to using snow areal depletion curves inferred from MODIS and its application to land surface modelling in Alaska. *Hydrological Processes*, Vol. 19, pp. 2755–2774. doi:10.1002/hyp.5784.
- Dyer, J. 2008. Snow depth and streamflow relationships in large North American watersheds. *Journal of Geophysical Research*, Vol. 113, No. D18113. doi:10.1029/2008JD010031.
- Goïta, K., Walker, A.E., and Goodison, B.E. 2003. Algorithm development for the estimation of snow water equivalent in the boreal forest using passive microwave data. *International Journal of Remote Sensing*, Vol. 24, No. 5, pp. 1097–1102.
- Goodison, B.E., and Walker, A.E. 1995. Canadian development and use of snow cover information from passive microwave satellite data. In *Passive Microwave Remote Sensing of Land-Atmosphere Interactions: Proceedings of the ESA/NASA International Workshop*. Edited by B.J. Choudhury, Y.H. Kerr, E.G. Njoku, and P. Pampaloni. VSP International Science Publishers, Utrecht, The Netherlands. pp. 245–262.
- Goodison, B.E., Rubinstein, I., Thirkettle, F.W., and Langham, E.J. 1986. Determination of snow water equivalent on the Canadian prairies using microwave radiometry. In *Modelling Snowmelt Induced Processes, Proceedings of the Budapest Symposium, 2–4 July 1986*, Budapest, Hungary. Edited by E.M. Morris. IAHS Publication 155, IAHS Press, Wallingford, U.K. pp. 163–173.
- Hornik, K., Stincombe, M., and White, H. 1989. Multilayer feedforward networks are universal approximators. *Neural Networks*, Vol. 2, pp. 359–366.
- Jain, S., and Lall, U. 2000. Magnitude and timing of annual maximum floods: Trends and large-scale climatic associations for the Blacksmith Fork River, Utah. *Water Resources Research*, Vol. 36, No. 12, pp. 3641–3651.
- Kelly, R.E.J., and Chang, A.T.C. 2003. Development of a passive microwave global snow depth retrieval algorithm for Special Sensor Microwave Imager (SSM/I) and Advanced Microwave Scanning Radiometer-EOS (AMSR-E) data. *Radio Science*, Vol. 38, No. 4, p. 8076. doi:10.1029/2002RS002648.
- Kurvonen, L., and Hallikainen, M. 1997. Influence of land-cover category on brightness temperature of snow. *IEEE Transactions on Geoscience and Remote Sensing*, Vol. 35, No. 2, pp. 367–377.
- Mote, P.W. 2006. Climate-driven variability and trends in mountain snowpack in western North America. *Journal of Climate*, Vol. 19, No. 23, pp. 6209–6220.
- Mote, P.W., Hamlet, A.F., Clark, M.P., and Lettenmaier, D.P. 2005. Declining mountain snowpack in western North America. *Bulletin of the American Meteorological Society*, Vol. 86, pp. 39–49. doi:10.1175/BAMS-86-1-39.
- Ramage, J.M., McKenney, R.A., Thorson, B., Maltais, P., and Kopynski, S.E. 2006. Relationship between passive microwave-derived snowmelt and surface-measured discharge, Wheaton River, Yukon Territory, Canada. *Hydrological Processes*, Vol. 20, pp. 689–704.
- Stewart, I.T., Cayan, D.R., and Dettinger, M.D. 2005. Changes towards earlier streamflow timing across western North America. *Journal of Climate*, Vol. 18, pp. 1136–1155.
- Tait, A., and Armstrong, R. 1996. Evaluation of SMMR satellite derived snow depth using ground-based measurements. *International Journal of Remote Sensing*, Vol. 17, No. 4, pp. 657–665.
- Tedesco, M., Pulliainen, J., Takala, M., Hallikainen, M., and Pampaloni, P. 2004. Artificial neural network-based techniques for the retrieval of SWE and snow depth from SSM/I data. *Remote Sensing of Environment*, Vol. 90, pp. 76–85.
- Tong, J., Déry, S.J., and Jackson, P.L. 2009. Topographic control of snow distribution in an alpine watershed of western Canada inferred from spatially-filtered MODIS snow products. *Hydrology and Earth System Sciences*, Vol. 13, pp. 319–326.

- Walker, A.E., and Goodison, B.E. 1993. Discrimination of a wet snow cover using passive microwave satellite data. *Annals of Glaciology*, Vol. 17, pp. 307–311.
- Yang, D., Robinson, D., Zhao, Y., Estilow, T., and Ye, B. 2003. Streamflow response to seasonal snow cover extent changes in large Siberian watersheds. *Journal of Geophysical Research*, Vol. 108, No. D18, p. 4578. doi:10.1029/2002JD003149.
- Yang, D., Zhao, Y., Armstrong, R., and Robinson, D. 2007. Streamflow response to seasonal snow cover mass changes over large Siberian watersheds. *Journal of Geophysical Research*, Vol. 112, No. F02S22. doi:10.1029/2006JF000518.
- Zhang, Q., Wang, C., Shinohara, F., and Yamaoka, T. 2007. Quasi-real time estimation of distributed precipitation using EOS/MODIS remote sensing dataset. In *Proceedings of the 2nd International Conference on Space Information Technology*, 10 November 2007, Wuhan, China. Edited by C. Wang, S. Zhong, and J. Wei. Proceedings of SPIE Volume 6795, The International Society for Optical Engineering, Bellingham, Wash. Paper 67957J-1.